EARTHQUAKE TSUNAMI INTERACTION DIAGRAM CONSIDERING FOUNDATION UPLIFT

Thanisorn SRIKULRUANGROJ[1], Atsushi MIKAMI[2]

[1]Student member of JSCE, Ph.D. Student, Dept. of Civil Eng., Tokai University
(4-1-1, Kitakaname, Hiratsuka-shi, Kanagawa 259-1292, Japan)
E-mail: 9LTAD004@cc.u-tokai.ac.jp

[2]Member of JSCE, Professor, Dept. of Civil Eng., Tokai University
(4-1-1, Kitakaname, Hiratsuka-shi, Kanagawa 259-1292, Japan)
E-mail: atsushi.mikami@tokai.ac.jp

Carey et al. developed earthquake-tsunami multihazard interaction diagram. This study extends their study by considering the foundation uplift as a limit state. Considering a three-story building supported by a mat foundation as a model, a ground motion recorded during the 2011 Tohoku earthquake and the tsunami hydrodynamic force were applied by variously changing their magnitude to make the diagram. The obtained earthquake-tsunami interaction diagram illustrates that the remaining resistance after the earthquake differs depending on the different levels of foundation uplift during the earthquake.

Key Words : *multihazard, nonlinear soil-structure interaction, foundation uplift*

1. INTRODUCTION

In the 2011 Tohoku earthquake, extensive tsunami damage occurred in the east coastal areas of Japan[1)]. Overturned buildings were found in the coastal area where is severely damaged by the tsunami[2),3)]. Yeh et al.[4)] suggested that the buildings were overturned by hydrodynamic force, buoyancy force, and soil instability. Latcharote et al.[5)] suggested that an overturning moment affected more by the buoyancy force than the hydrodynamic force; however, the decisive factors that led the building to overturn are still under investigation. Mimura et al.[6)] and H. Gokon et al.[7)] showed the damaged structures in the coastal area that suffered from the sequential earthquake and tsunami during the 2011 Great East Japan Earthquake and Tsunami events. Since structures were severely shaken by the earthquake and were further damaged by the subsequent huge tsunami, a method of describing the effects of sequential multihazard (earthquake-tsunami) is necessary.

This kind of damage accumulation problem also occurs when major earthquakes occur successively, such as the 2016 Kumamoto earthquake[8)]. Ribeiro et Al.[9)] proposed a framework to consider the post-mainshock earthquake sequential. The results showed that a failure of a structure by considering mainshock-aftershock sequences increased significantly by comparison with only a single mainshock event.

Regarding earthquake and tsunami multihazard, Carey et al.[10)] proposed a framework to illustrate the effects of the earthquake and tsunami sequence on the soil-foundation-bridge system. Scott and Mason[11)] illustrated that amplification factors from the sequential earthquake and tsunami loading led to more intensity measures than under only an earthquake. Carey et al.[12)] proposed an earthquake-tsunami interaction diagram for predicting effects of the sequential earthquake-tsunami multihazard on a bridge. As Carey suggested[12)], a multihazard interaction diagram is very useful because it enables to show that the residual effects of earthquake loading on the structure reduce resistance to subsequent tsunami loading. Extending Carey's work, this study further develops the earthquake-tsunami interaction diagram considering foundation uplift on a building structure being subjected to a strong ground motion.

2. ANALYSIS FRAMEWORK

(1) Analysis framework

This study basically follows the multihazard analysis framework developed by Carey et al.[12)]; however, further development of the analysis was conducted so that it can take foundation uplift into account. Explanation of the framework will be given in three stages below.

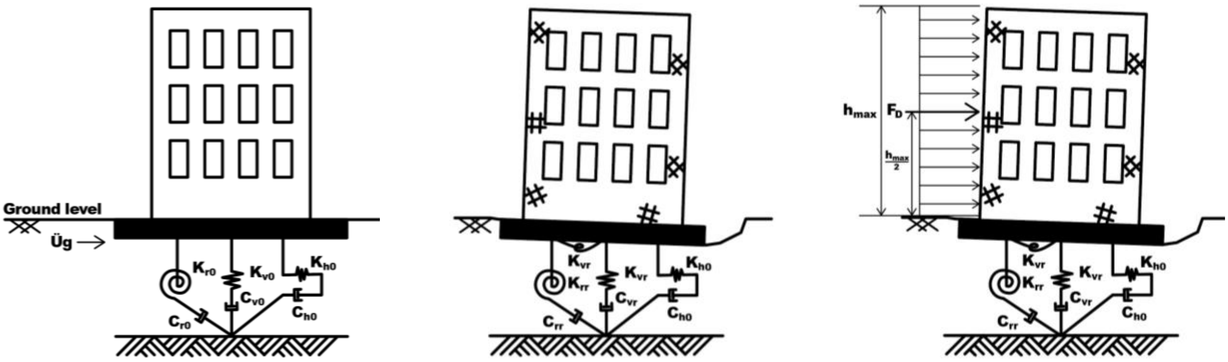

a) earthquake loading **b)** preparation before a tsunami **c)** tsunami loading

Fig. 1 Analysis framework of three stages

a) Stage 1: Earthquake ground motion loading

In the first stage, the earthquake ground motion is given to a shallow foundation at the ground surface level. For the discussion of foundation uplift, three degrees of freedom for the foundation are considered in this study. The soil-foundation system is modeled as a rigid foundation supported by springs and dashpot. The springs and dashpots represent the compliant soil-foundation system's stiffness and damping characteristics, as shown in **Fig.1a)**. The method to determine parameters of the soil-foundation system will be described in chapter 3.

b) Stage 2: Before a tsunami loading

In the second stage, the structure is described as the initial condition with its damaged/deformed state by the earthquake before a tsunami loading. When the foundation rotation is significantly large, the induced vertical motion needs to be considered as the coupling of rotational and vertical degrees of freedom, as shown in **Fig. 1b)**.

c) Stage 3: Tsunami loading

Although the tsunami loading is hydrodynamic force, this study treated it as static force, following the paper by Carey et al.[12)]. The hydrodynamic pushover analysis is conducted in the third stage. According to ASCE/SEI 7-16[16)], the hydrodynamic force is statically applied to the whole structure from the ground surface level to the specific tsunami inundation depth, h. The tsunami flow velocity is estimated as uniform throughout the tsunami height; hence, the hydrodynamic pressure has been distributed as a uniform load. By assuming the tsunami inundation depth, h_{max}, the resulting hydrodynamic force has applied at the center of the tsunami height, as indicated in **Fig. 1c)**. The intensity of the hydrodynamic force is increased by increasing the tsunami flow velocity, u, incrementally in a nonlinear pushover analysis[17)].

Carey et al.[12)] proposed the earthquake-tsunami multihazard interaction diagram that consists of the spectral acceleration, S_a, and the hydrodynamic force, F_D, on the ordinate and abscissa axis, respectively, for predicting the defined limit state. This approach was taken in this study.

(2) Limit state

ASCE/SEI 7-10[18)] states that beyond which the structure becomes unsuitable for service or unsafe as a limit state. Since this study considers the effects of sequential earthquake and tsunami, a limited state could be interpreted as the failure of the structure caused by any of the two hazards (i.e., the earthquake or the tsunami) or both, as Carey et al.[12)]. According to the Performance-Based Design (PBD) concept[19)], the amount of deformation in some structures should be considered to verify the structure will be safe or unsafe. Therefore, this study defined the degree of foundation uplift (i.e., ground contact ratio or rotation deformation of foundation) as the limit state.

3. ANALYTICAL MODEL

(1) Building model

From the observation data[2),3)], The overturned buildings by the Tohoku tsunami event are mostly the low-rise building on a shallow foundation. Therefore, this study considered a three-story building on the mat foundation, as shown in **Fig. 2**. This study model

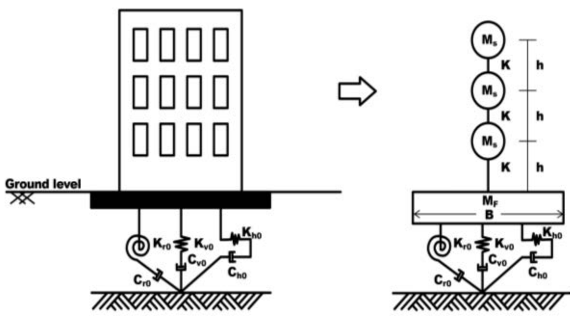

Fig. 2 A three-story building into three-story lumped mass model

Table 1 Parameters for model analysis

Parameters	Value
Lumped mass, M_S (ton)	200
Foundation mass, M_F (ton)	100
Height, H (m)	3.5
Young modulus, E (kN/m^2)	2 x 10^8
Moment of inertia, I (m^4)	0.018
Cross section area, A (m^2)	1
Damping coefficient of the structure, η	0.05

a structure by lumped mass and beam element. Each story and foundation was represented by three degrees of lumped mass (i.e., the total degrees of freedom in this structure are 12 degrees) was considered. **Table 1** summarizes the parameters for a typical three-story building used to analyze in this study.

(2) The soil foundation system

Parameters of the soil-foundation system, including the spring and dashpot in the vertical, the horizontal, the rotational direction, are shown in **Fig. 2**. Parameters of the soil-foundation system can be calculated by Equation (1) – Equation (7) proposed by Gazetas[20] by assuming ground density, ρ = 1,800 kg/m^3; Poisson's ratio, $\nu = 0.4$; Coefficient indicating the frequency dependence of damping vertical and rotational $\overline{C}_v = 0.9$ and $\overline{C}_r = 0.2$, respectively. Two kinds of soil conditions are prepared in this study. Thus, this study assumes shear wave velocities of two kinds of soil, V_s = 300 m/s and V_s = 1000 m/s.

$$K_{v0} = \frac{4.54G(B/2)}{1-\nu} \quad (1)$$

$$K_{h0} = \frac{9G(B/2)}{2-\nu} \quad (2)$$

$$K_{r0} = \frac{3.6G(B/2)^3}{1-\nu} \quad (3)$$

$$C_{v0} = \rho V_{LA} A \overline{C_v} \quad (4)$$

$$C_{h0} = \rho V_s A \quad (5)$$

$$C_{r0} = \rho V_{LA} I \overline{C_r} \quad (6)$$

$$V_{LA} = \frac{3.4}{\pi(1-\nu)} V_S \quad (7)$$

(3) Soil-structure interaction model

TDAP III program was used for the calculation of structural responses against multihazards considering foundation uplift in this study. Following explanations are given by referring to TDAP III manual[21),22], especially about foundation uplift. TDAP III treats the foundation-soil system as a rigid foundation supported by springs. The geometric nonlinearity associated with foundation uplift is considered in the stiffness and damping of the rotational spring at the foundation evaluated based on elastic wave theory. Analysis methods of foundation uplift depend on the ground contact ratio. Ground contact ratio, η, and overturning moment, M can be computed by Equation (8) and Equation (11), respectively.

$$\eta = 3\left(\frac{1}{2} - \frac{M_{\max}}{WL}\right) \quad (8)$$

$$\frac{M}{M_0} = \left(3 - 2\sqrt{\frac{\theta_0}{\theta}}\right) \quad (9)$$

$$\theta_0 = \frac{M_0}{K_{r0}} \quad (10)$$

$$M_0 = \frac{WL}{\alpha} \quad (11)$$

Where W is the building weight; L is the foundation width; θ is the rotation deformation; the coefficients according to the distribution of ground reaction forces, $\alpha = 6$; and θ_0 and M_0 is the uplift limit rotation deformation and the uplift limit overturning moment, respectively. The seismic response analysis methods are classified into three kinds based on the degree of foundation uplift, as described in **Table 2**.

4. EARTHQUAKE AND TSUNAMI LOADING

(1) Earthquake ground motion

A subduction-zone earthquake ground motion was selected from the KiK-net stations recorded at the IWTH23 station (38.103° N 142.860° E) during the 2011 Tohoku earthquake. The acceleration time history for the east-west (EW) component and the elastic spectrum acceleration response are shown in **Fig. 3a)**. and **Fig. 3b).** The peak ground acceleration

Table 2 Classification of analytical methods by ground contact ratio[22]

Ground contact ratio, η	Analysis Method
η ≥ 75%	Linear seismic response analysis
η ≥ 65%	Nonlinear seismic response analysis by considering uplift nonlinearity in rotational spring of the ground
η ≥ 50%	Uplift nonlinear seismic response analysis that can account for induced vertical motion

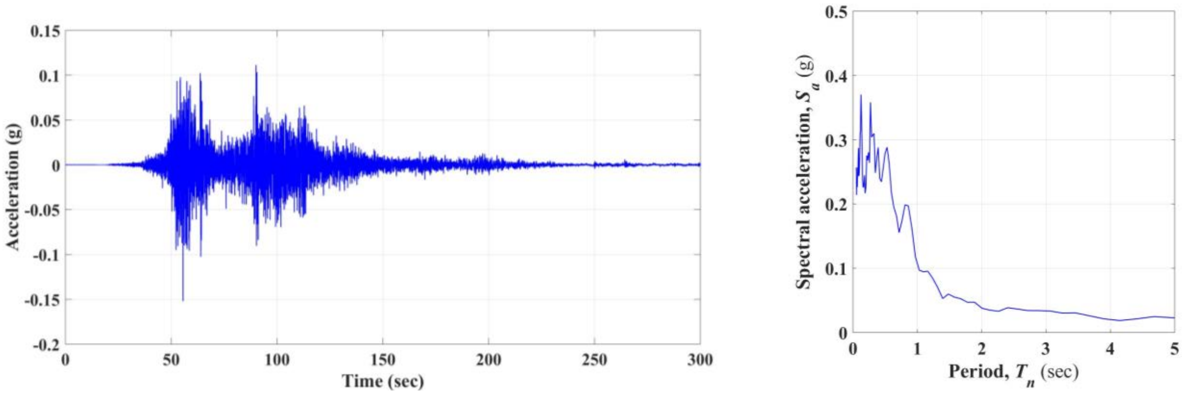

a) acceleration time history **b)** response spectrum

Fig. 3 Earthquake ground motion recorded during the 2011 Tohoku earthquake at IWITH 23 station

(PGA) is 0.15 g. Spectral acceleration, $S_{a,}$ is calculated by assuming 5% damping. This ground motion is used by varying its amplitude variously to make the interaction diagram. As mentioned, TDAP allows to define three kinds of contact ratio as limit state, this study calculates interaction diagram for each limit state to examine whether the remaining resistance after the earthquake differs depending on the different levels of foundation uplift during the earthquake.

(2) Tsunami Force

By following the paper by Carey et al.[12], this study focuses on the hydrodynamic force, F_D, which is one of the main causes of overturned buildings[4),5)]. By assuming the drag coefficient, C_D = 2, as described in FEMA 2012[23)], the building width that the tsunami impact, B = 5 m; the fluid density, ρ = 1,000 kg/m^3. and $(hu^2)_{\max}$ is the maximum of the momentum-flux, where h is the tsunami inundation depth; and u is the tsunami flow velocity. Therefore, the hydrodynamic force applied to the structure can be computed by Equation (12), as illustrated in **Fig. 1c**.

$$F_D = \frac{1}{2} C_D \rho B (hu^2)_{\max} \tag{12}$$

5. COMPUTATIONAL RESULTS

Two examples of the rotation deformation of foundation and ground contact ratio-time histories are shown in **Fig. 4** and **Fig. 5**, respectively. **Fig. 4a** and **Fig. 5a** present the response and ground contact ratio for a case where the tsunami via hydrodynamic force reached the limit state. The case in which the limit state are reached by the earthquake is presented in **Fig. 4b** and **Fig. 5b**. It is found that the rotational displacement of the foundation is more responsive and becomes larger due to foundation uplift for the large earthquake cases. The earthquake-tsunami interaction diagrams for two different tsunami heights and two different shear wave velocities are presented in **Fig. 6**. The results show the earthquake ground motion reached the limit state, resulting in a drastic reduction in the interaction diagram (i.e., the hydrodynamic force is not required to reach the limit state). However, if the defined limit state is not reached by earthquake ground motion, the following tsunami will reach the limit state. **Fig. 6** illustrates that the tsunami flow velocities are between 2 m/s to 4 m/s when the tsunami heights are 7 and 14 meters for two soil types, respectively, to reach the prescribed limit state by the following tsunami. It is found that the remaining resistance after the earthquake differs depending on the different levels of foundation up-lift during the earthquake. Note that since the ground contact ratio is little affected by soil stiffness, the tsunami flow velocity, which reached the limit state of the stiff soil, is similar to that of hard rock, as Equation (8).

6. CONCLUSIONS

Following the multihazard interaction diagram proposed by Carey et al., this study extended the earthquake-tsunami interaction diagram to consider nonlinear soil-structure interaction with foundation uplift. A three-story building supported by a mat foundation was considered, and a recorded ground motion during the 2011 Tohoku earthquake (EW component) at the IWTH23 station and the hydrodynamic force were applied as an earthquake and a tsunami loading, respectively. As with the Carey's work, the results interestingly showed the residual effects of earthquake loading on the structure reduce resistance to subsequent tsunami loading. It was also found that the remaining resistance after the earthquake differs depending on the different levels of foundation uplift during the earthquake.

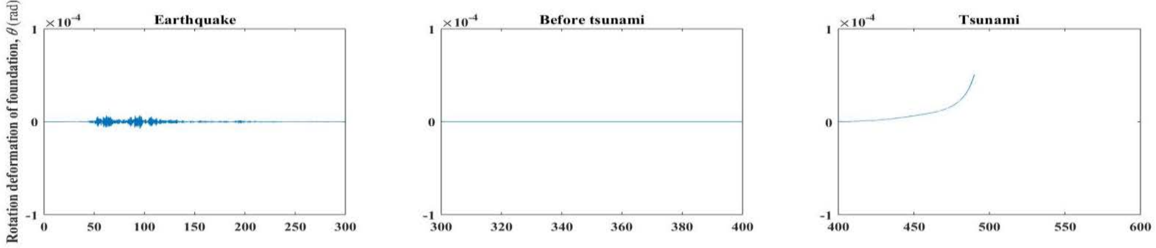

a) the prescribed limit state was reached by the tsunami

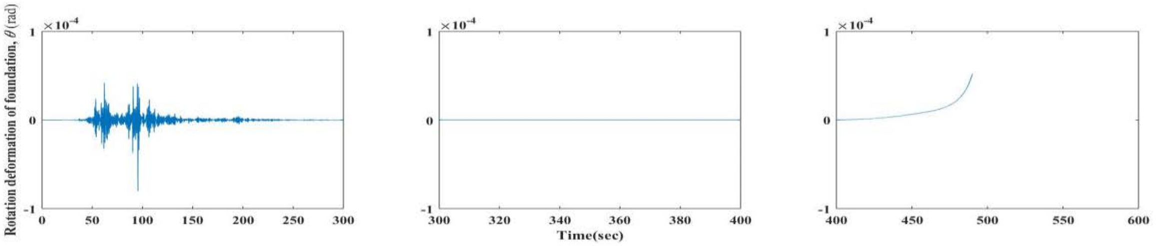

b) when the earthquake motion reached the prescribed limit state.
Fig. 4 Foundation response's time history for sequential earthquake-tsunami multihazard

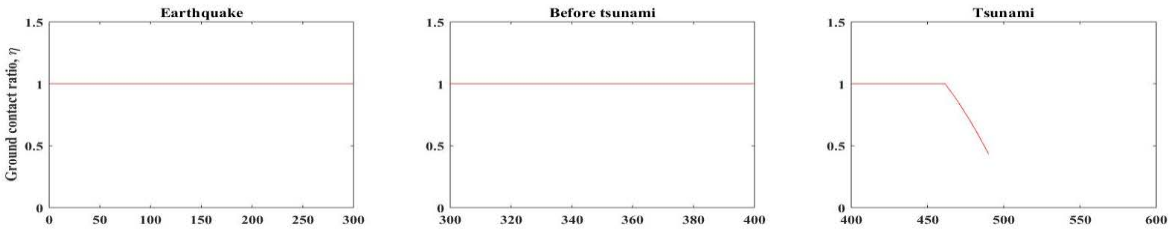

a) the prescribed limit state was reached by the tsunami

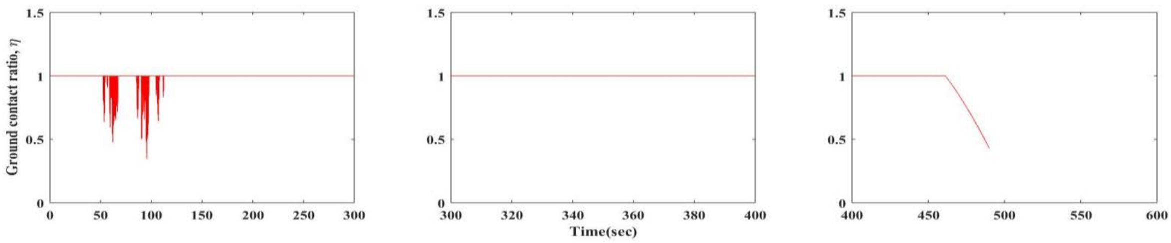

b) when the earthquake motion reached the prescribed limit state.
Fig. 5 Ground contact ratio's time history for sequential earthquake-tsunami multihazard

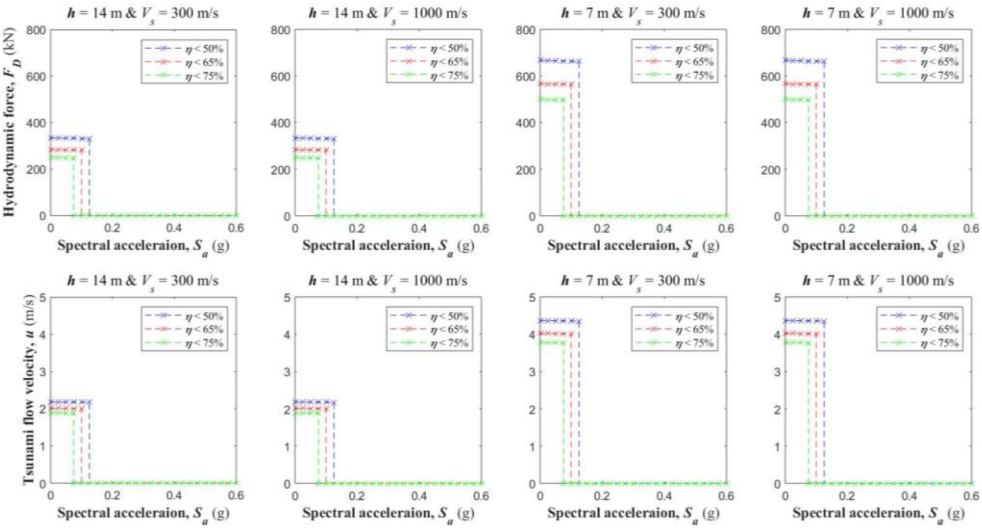

a) **b)** **c)** **d)**

Fig. 6 Interaction diagrams of hydrodynamic force and tsunami velocity with ground motion earthquake (IWTH23): a) tsunami height = 14 m and V_s = 300 m/s; b) tsunami height = 14 m and V_s = 1000 m/s; c) tsunami height = 7 m and V_s = 300 m/s; d) tsunami height = 7 m and V_s = 1000 m/

ACKNOWLEDGMENT: The authors would like to express our special thanks of gratitude to the National Research Institute for Earth Science and Disaster Prevention (NIED) for the ground motion data. We also appreciate Dr. Kashima (International Institute of Seismology and Earthquake Engineering, BRI) for providing the software View-Wave to calculate spectral acceleration. We also would like to thank Mr. Soichiro Akiyama, an undergraduate student of Tokai University, for his support regarding Japanese for the 2011 Tohoku earthquake-tsunami events data.

REFERENCES

1) Kazama, M. and Noda, T. : Damage statistics (Summary of the 2011 off the Pacific Coast of Tohoku Earthquake damage), *Soil and Foundations*, Vol. 52, No.5, pp.780-792, 2012.
2) Nishiyama, I., Okawa, I., Fukuyama, H. and Y. Okuda : Building damage by the 2011 off the Pacific coast of Tohoku earthquake and coping activities by NILIM and BRI collaborated with the administration, UJNR, 2011.
3) Suppasri, A., Shuto, N., Imamura, F., Koshimura, S., Mas, E. and Yalciner, A. C. : Lessons learned from the 2011 Great East Japan tsunami: performance of tsunami countermeasures, coastal buildings, and tsunami evacuation in Japan, *Pure Appl. Geophys*., 170, pp. 993-1018, 2013.
4) Yeh, H., Sato, S., and Tajima, Y : The 11 March 2011 East Japan earthquake and tsunami: tsunami effects on coastal infrastructure and buildings, *Pure Appl. Geophys*., 170, pp. 1019-1031, 2013.
5) Latcharote, P., Suppasri, A., Yamashita, A., Adriano, B., Koshimura, S., Kai, Y. and Imamura, F. : Possible Failure Mechanism of Buildings Overturned during the 2011 Great East Japan Tsunami in the Town of Onagawa, *Front. Built Environ. Earthquake Engineering*, Vol. 3, 2017.
6) Mimura, N., Yasuhara, K., Kawagoe, S., Yokoki, H., Kazema, S. : Damage from the great east Japan earthquake and tsunami — a quick report, Vol. 16, pp. 803–818, 2011.
7) Gokon, H. and Koshimura, S.: Mapping of building damage of the 2011 Tokoku Earthquake Tsunami in Miyagi prefecture, *Coastal Engineering Journal*, Vol. 54, No. 1, 2012.
8) Goda, K., Campbell, G., Hulme, L., Ismael, B., Ke, L., Marsh, R., Sammonds, P., So, E., Okumura, Y., Kishi, N., Koyama, M., Yotsi, S., Kiyono, J., Wu, S. and Wilkinson, S. : The 2016 Kumamoto earthquake: cascading geological hazards and compounding risks, *Front. Built Environ Earthquake Engineering*, Vol.2, 2016
9) Ribeiro, F. L. A., Barbosa, A. R. and Neves, L. C. : Application of reliability-based robustness assessment of steel moment resisting frame structures under post-mainshock cascading events, *J. Struct.Eng. (140)*, A4014008, 2014.
10) Carey, T., Mason, H. B., Barbosa, A. R. and Scott, M.H. : Modeling framework for soil-bridge system response during sequential earthquake and tsunami loading, *Proceedings of the 10th National Conference in Earthquake Engineering*, 2014.
11) Scott, M. H. and Mason, H. B.: "Constant-ductility response spectra for sequential earthquake and tsunami loading., *Earthquake Engng. Struct. Dyn.*, 46, pp. 1549-1554, 2017.
12) Carey, T. J., Mason, H. B., Barbosa, A. R. and Scott, M.H. : Multihazard earthquake and tsunami effects on soil-foundation-bridge system, *J. Bridge Eng., 24(4)*, 04019004-1, 2019.
13) Hayashi, Y.: Damage reduction effect due to base mat uplift of buildings, *J.Struct. Constr. Engng*., 485, pp.53-62, 1996. (In Japanese)
14) Hayashi, Y., Tamura, K., Mori, M. and Takahashi, I.: Simulation analyses of buildings damaged in the 1995 Kobe, Japan, earthquake considering soil-structure interaction, *Earthquake engng. Struct. dyn*., 28, pp. 371-391, 1999.
15) Iwashita, K. and Taniguchi, H.: Effect of uplift on earthquake response of building, *The 12th world conference of Earthquake Engineering,* 2000.
16) ASCE.: Minimum design loads and associated criteria for buildings and other structures, *ASCE/SEI 7-16*., 2016.
17) Vamvastsikos, D. and Cornell, C. A. : Incremental dynamic analysis, *Earthquake Engng Struct. Dyn.*, Vol. 31, pp.491-514, 2002.
18) ASCE.: Minimum design loads and associated criteria for buildings and other structures, *ASCE/SEI 7-10*., 2010.
19) Honjo, Y., Kikuchi, Y. and Shirato, M. : Development of the design codes grounded on the performance based design concept in Japan; *Soil and Foundations*, Vol. 50, No. 6, pp.983-1000,2010.
20) Gazetas, G.: *Foundation Engineering Handbook (second edition, ed. By Fang, H.Y.)*, Chapter 15, Van Nostrand Reinhold, 1991.
21) TDAP III batch version user's guide version 3.09, ARK Information Systems, INC, 2017. (In Japanese)
22) Nuclear standard committee of JEA: Technical regulations for seismic design of nuclear power plants, *JEAC 4601-2008*, pp.181-186, 2009. (In Japanese)
23) FEMA: Guidelines for design of structures for vertical evacuation from tsunamis, *FEMA P-646 Second Edition*, 2012.

(Received July 1, 2009)
(Accepted November 1, 2009)